Proceedings of the Sixth International Conference on
Railway Technology: Research, Development and Maintenance
Edited by: J. Pombo
Civil-Comp Conferences, Volume 7, Paper 9.4
Civil-Comp Press, Edinburgh, United Kingdom, 2024
ISSN: 2753-3239, doi: 10.4203/ccc.7.9.4

Surface Damage Assessment in Rail and Wheel Steels Using an Innovative Vision System

A. Mazzu, I. Bodini, N. Zani, L. Ghidini, C. Petrogalli, S. Bonometti, G. Coffetti and D. Palandi

**Department of Mechanical and Industrial Engineering,
University of Brescia
Italy**

Abstract

Rolling-sliding tests were done by a bi-disc machine on specimens realised by two different railway wheel steels (SUPERLOS® and ER8), coupled with the same rail steel (900A). Varying contact load and sliding speed were applied, up to very severe working conditions. Weight loss and coefficient of friction were monitored during the tests. At the end of the tests, the surface state was evaluated by roughness measurements obtained by an innovative laser distance sensor. Wear severity was evaluated in terms of specific T-gamma and Archard coefficients.

The results showed that, with increasing load and sliding speed, there is a sudden transition from mild or severe wear to catastrophic wear. This is correlated with both parameters, but the sliding speed showed a stronger effect. The roughness at the test end is strongly correlated with the sliding speed. Among the wheel steels, the SUPERLOS® showed a better performance than the ER8; the rail steel showed better performance than the wheel steels, rarely being subjected to catastrophic wear.

These tests showed the capability of the experimental set-up to simulate very severe wear regimes, whereas the innovative vision system showed its potential as a damage evaluation tool in rolling contact tests.

Keywords: rolling contact tests, rail-wheel steels, laser distance triangulation, coefficient of friction, wear, roughness.

1 Introduction

High contact pressure and slip speed can occur at the wheel-rail interface, especially in severe conditions such as curving, braking or slipping. In particular, pressures up

to 1500 MPa and sliding speeds exceeding 0.1 m/s are documented in the literature [1-3]. Both contacting bodies can be seriously damaged in such conditions, especially by wear and ratcheting [4, 5]. Investigating the material response under high pressure and sliding is crucial to address the correct procedure to prevent or limit such damage.

A diffused way to evaluate the material performance is based on the wear maps, which give the wear rate as a function of the load and of the sliding speed, where the wear rate is evaluated according to the Archard model. Wear maps are given for several materials employed in railway applications [6-8]. Such maps are usually obtained by experimental tests, carried out by means of disc-to-disc or pin-on-disc machines, with the latter mainly used when high sliding speeds are applied. Based on the wear rate, the wear regime can be classified as "mild", "severe" or "catastrophic", characterized by different damage mechanisms. In mild wear surface oxidation is the main wear mechanism, whereas severe and catastrophic wear are characterised by surface cracking and spalling [6]. The resulting surface appearance is strictly correlated with the wear regime. The transition from a wear regime to another, in operation, can be due to non-exceptional changes in the running conditions; therefore, addressing the wear behaviour in severe operating condition is crucial to prevent serious damage.

In this paper, the wear behaviour of two railway wheel steels, coupled with the same rail steel, is investigated in varying working conditions by means of disc-to-disc experiments, even in the range of sliding speed where usually pin-on-disc machines are used. The response of both rail and wheel materials is evaluated in terms of the T-gamma and Archard models, identifying especially the conditions leading to catastrophic wear. The surface state determined by the occurred damage are evaluated by an innovative vision system, based on laser triangulation, which allows measuring various surface parameters such as roughness and shape alterations. A correlation between these parameters and the wear regime is searched.

2 Methods

Rolling and sliding contact tests were carried out by means of a bi-disc machine, whose schematic is shown in Figure 1. The specimens were discs with a diameter of 60 mm and thickness of 15 mm, obtained from real rails and wheels. In each test, a wheel specimen was coupled with a rail one. The rail steel was of 900A quality for all the couplings. For the wheel specimens, two steels were used: EN 13262 ER8 grade steel, and a Silicon and Manganese Carbon steel with peculiar pearlitic microstructure, developed by LucchiniRS and commercially branded as SUPERLOS®, approved by railway standards such as BS 5892-3:1992+A2:2009 (as RS8T) and EN 13262 as ERS8. The wheel specimens were mounted as followers and the rail ones as drivers.

The working conditions are summarized in Table 1, where $P0$ is the Hertz contact pressure, k is the cyclic shear yield stress of the wheel steel, Vs the sliding speed, n average rolling speed, and c is the creepage, e.g. the ratio of the sliding speed to the average tangential speed of the specimens.

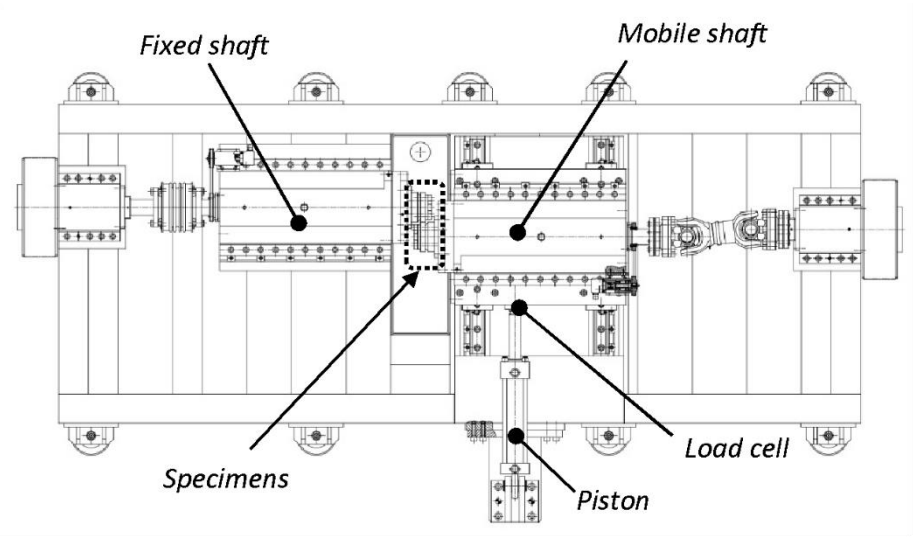

Figure 1: Schematic of the bi-disc machine.

Pressure ratio P0/k	Sliding speed Vs = m/s	Rolling speed n = r. p. m.	Creepage c = %
2	0.05	500	3.2
2	0.1		6.4
2	0.2		12.8
2	0.3		19.2
4	0.05		3.2
4	0.1		6.4
4	0.2		12.8
5	0.1		6.4
5	0.2		12.8

Table 1: Working conditions in the wear tests.

The maximum duration of the test was set to 60.000 cycles unless excessive damage forced an earlier end. Before the tests, each specimen couple was subjected to a run-in phase of 5000 cycles with $P0/k = 2$ and $c = 1\%$, to induce a reciprocal adaptation of the contact surfaces before imposing the target sliding speed. During the tests, the mobile shaft torque and the piston force were monitored and recorded; from these, the coefficient of friction was calculated.

Every 20.000 cycle, and at the end of the test anyway, the specimens were weighed by means of a 0.001 g precision balance, to determine the weight loss. Subsequently, the contact surface was acquired by a 2D/3D profile sensor Wenglor MLWL171, which allows determining the surface profile by the laser triangulation method (see Figure 2). A laser blade is projected onto the target object. The integrated camera acquires the blade deformed by the target profile; the software elaborates it accounting for the angle between the camera and the blade, thus obtaining the precise profile of the target surface. The used sensor allows obtaining 6.000 profiles per second at most,

with 2.048 points per profile. To determine the angular position of the acquire profile, a specifically designed analogic linear encoder was employed. This is an axial cam, with maximum diameter of 50 mm and minimum diameter of 44 mm; the height of the part with maximum diameter varies linearly with the angle, from 3 to 8 mm. The encoder rotated with the specimen and was mounted always in the same position with respect to it, this way allowing determining the angular position of the acquired profile. In Figure 2, the reference directions are shown: radial (z) and axial (y).

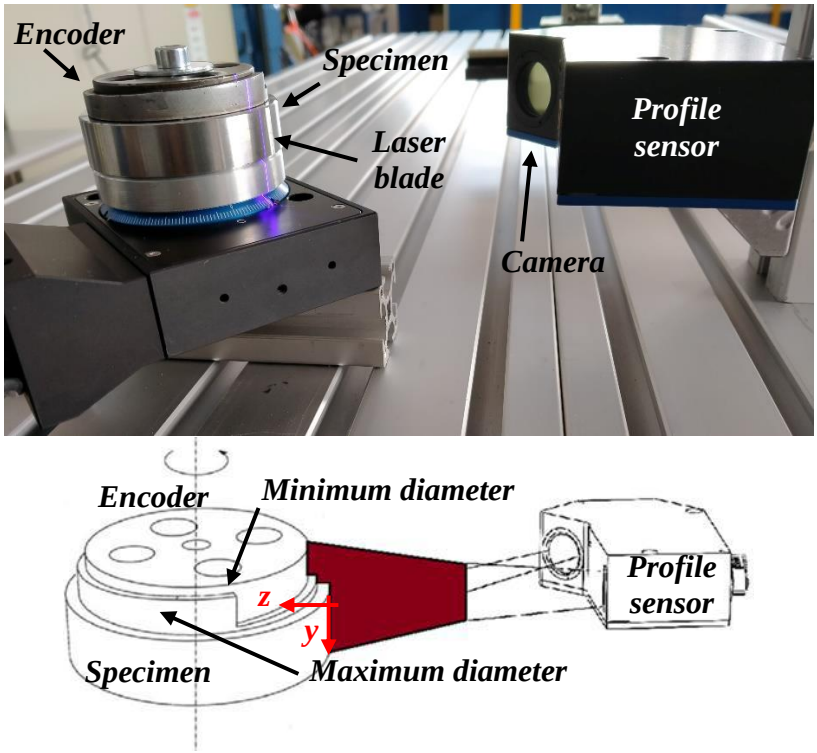

Figure 2: Set-up of the 3D profile sensor and acquisition principle.

Figure 3 shows the superposition of 5 typical acquired profiles of the wheel specimen: by qualitatively analyzing them, the region of effective contact with the coupled specimen could be identified as the region of interest (delimited by the blue lines in the figure) and isolated from the rest; the same region of interest was taken on the coupled rail specimen.

Once the profiles were determined, the quadratic roughness Ra had to be calculated. However, a preliminary elaboration was necessary to avoid a measurement error related to the average slope of the profile: the linear regression line of the considered profile was calculated and, if its slope exceeded 0.8°, it was roto-translated as shown in Figure 4.

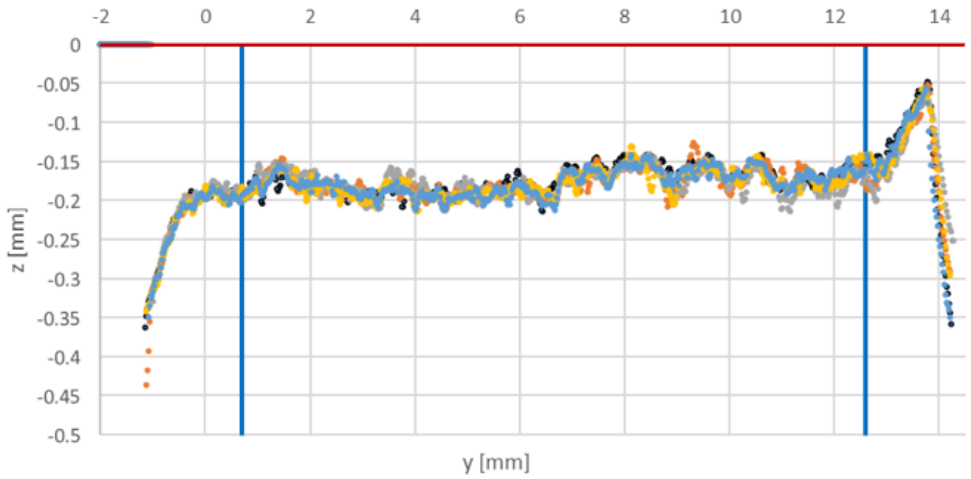

Figure 3: Superposition of 5 acquired profiles and identification of the region of interest.

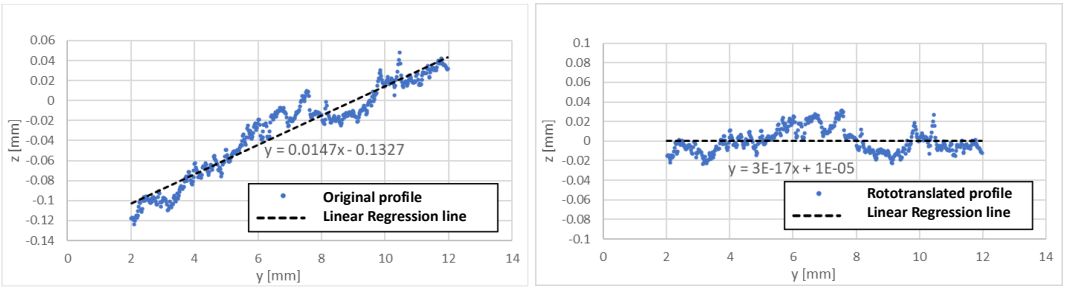

Figure 4: Roto-translation of the acquired profile.

3 Results

Given the particularly severe working conditions, only in a few cases the maximum loading cycles could be applied; in most cases, the tests were early stopped owing to the excessive specimen damage. As the tests on the SUPERLOS® were done after the ones on the ER8, the duration of the tests on the SUPERLOS® was set as the same as the duration of the corresponding tests on the ER8, except for the one with $P0/k = 5$ and $Vs = 0.2$ m/s, which was interrupted earlier due to excessive damage. The duration of the tests is reported in Figure 5.

To comment the behaviour of the coefficient of friction in the tests, an explicative example is given in Figure 6, where the results of two tests on the ER8 steel are shown, with $Vs = 0.05$ m/s for both, and $P0/k$ assuming the value of 2 and 4, respectively. With $P0/k = 2$ the coefficient of friction stabilizes around the value of 0.5; with $P0/k = 4$, after an initial transitory where the behaviour is comparable to the previous one, the coefficient of friction stabilizes around 0.1. This suggests that the increment of the normal and tangential loads is not proportional. Possible reasons for this can be the following:

- The tangential load is related to local interlocking between asperities rather than to the overall stress state;

- With higher pressure, more wear debris is formed, which tends to separate the contacting bodies;
- With higher pressure, more vibration is induced into the system, therefore the contact between the bodies is not continuous and the measured torque is, on average, lower.

A similar trend was observed even in the other tests.

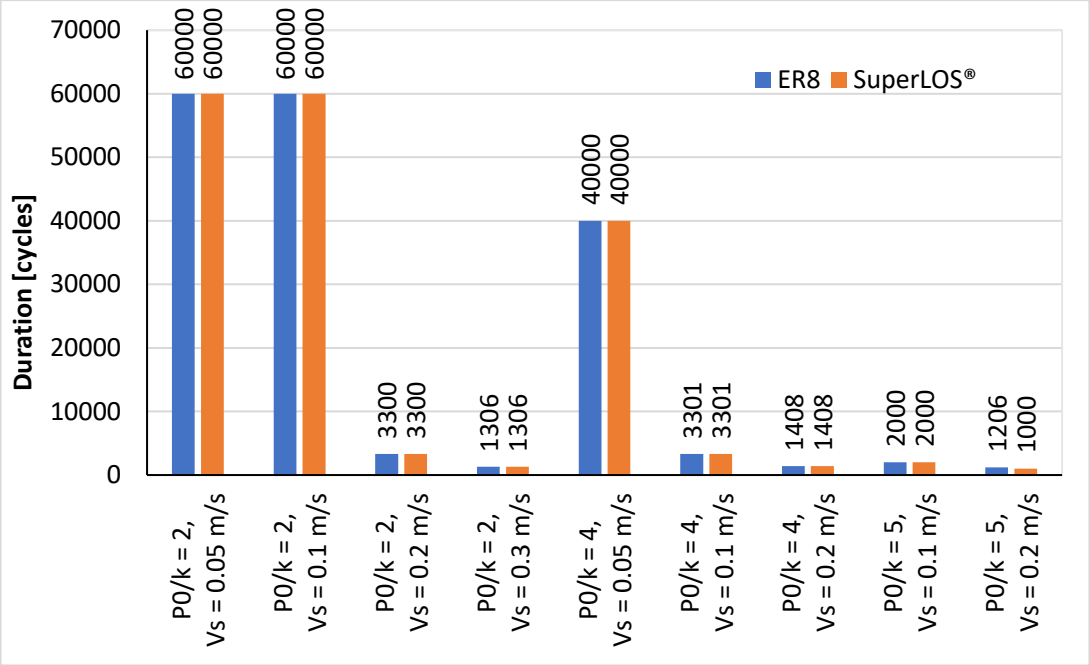

Figure 5: Duration of the tests.

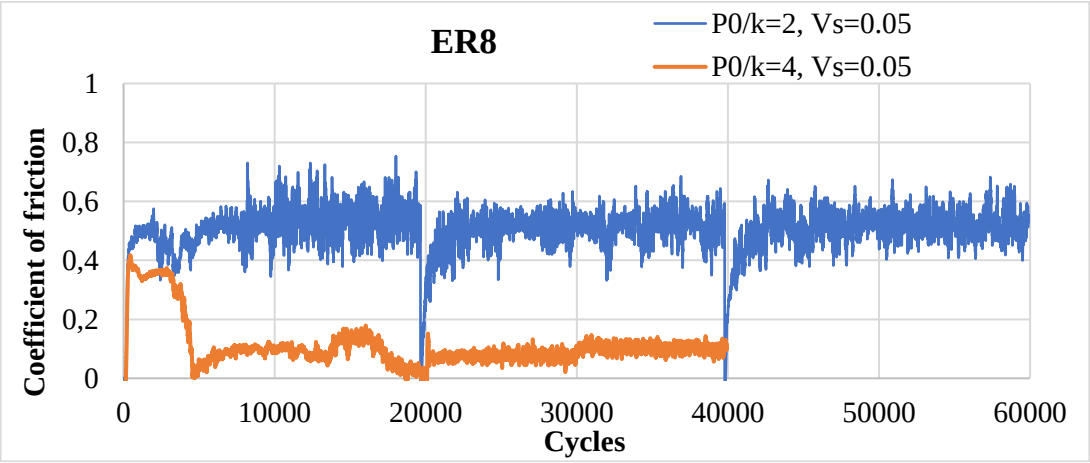

Figure 6: Coefficient of friction in the tests on the ER8 steel with $Vs = 0.2$ m/s and two different values of $P0/k$.

The surface aspect of the specimens at the end of the tests is shown in Figure 7 for the ER8; similar results were obtained for the SUPERLOS® specimens. In the least severe condition ($P0/k = 2$, $Vs = 0.05$ m/s) the surface exhibited the typical corrugations due to stick-slip phenomena, as found even in previous test campaigns

[9, 10]. With increasing rolling speed, the corrugations disappeared and the surface became rougher. With increasing contact pressure, macroscopic plastic deformation areas appeared, leading to the loss of cylindricity, in some cases up to poligonalization.

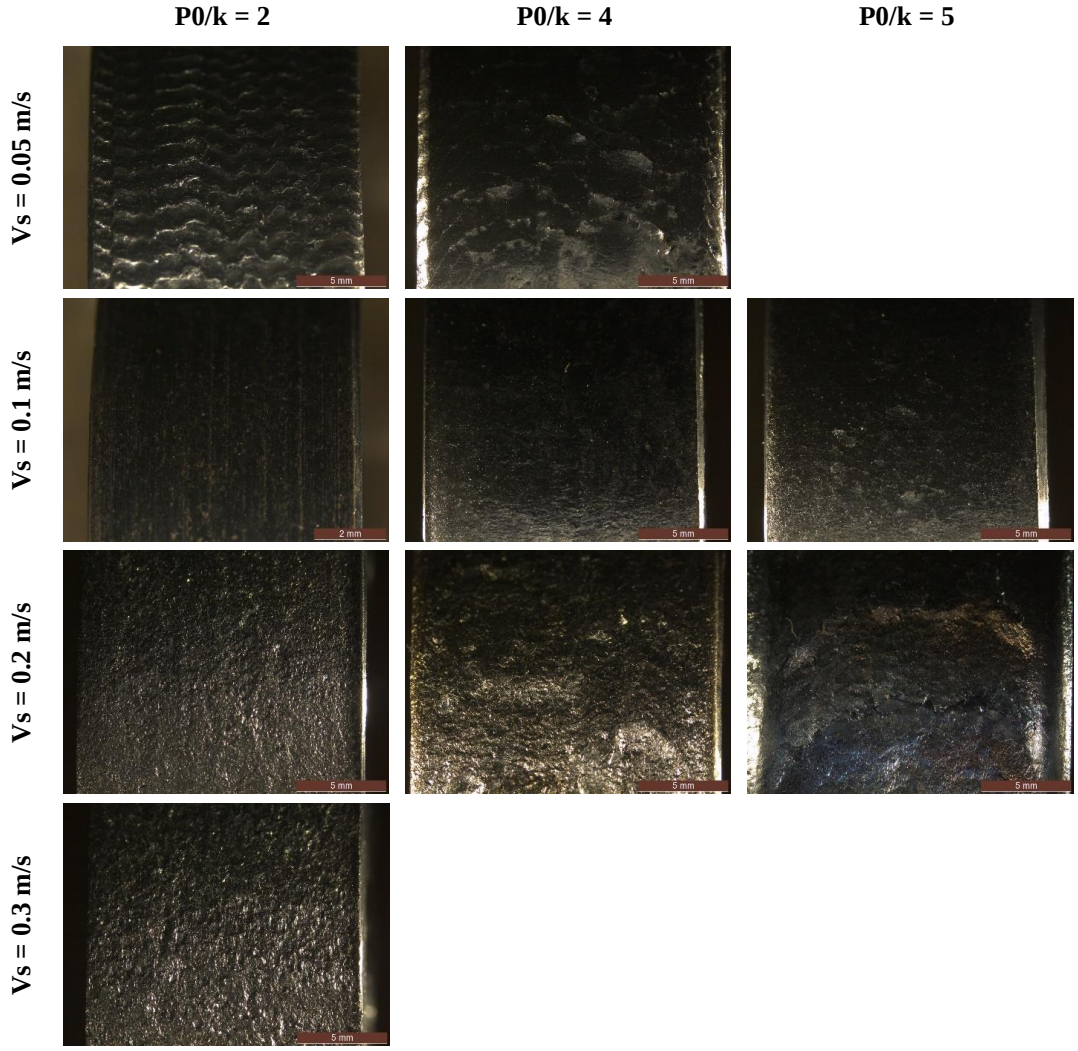

Figure 7: Surface aspect of the ER8 specimens at the end of the tests.

The roughness analyses with the profile sensor were done both for the wheel and the rail specimens. The circumference of each specimen was divided into 36 sectors of 10° each. In each sector, various profiles were acquired and the quadratic roughness Ra was calculated for each of them; the average Ra value of all profiles belonging to the same sector was assigned as the characteristic Ra of that sector. In Figure 8 the variation of Ra in the wheel specimens with the angular position of the examined sector is shown; in Figure 9 the same quantity for the rail specimens is shown. The highest Ra values are associated with the highest sliding speed, with a trend overall increasing with increasing contact pressure. Overall, the roughness values are higher in the ER8 specimens than in the corresponding SUPERLOS® ones. In the tests with

the ER8 the roughness is higher in the wheel specimens than in the rail ones; in the tests with the SUPERLOS® the are no remarkable differences between wheel and rail specimens.

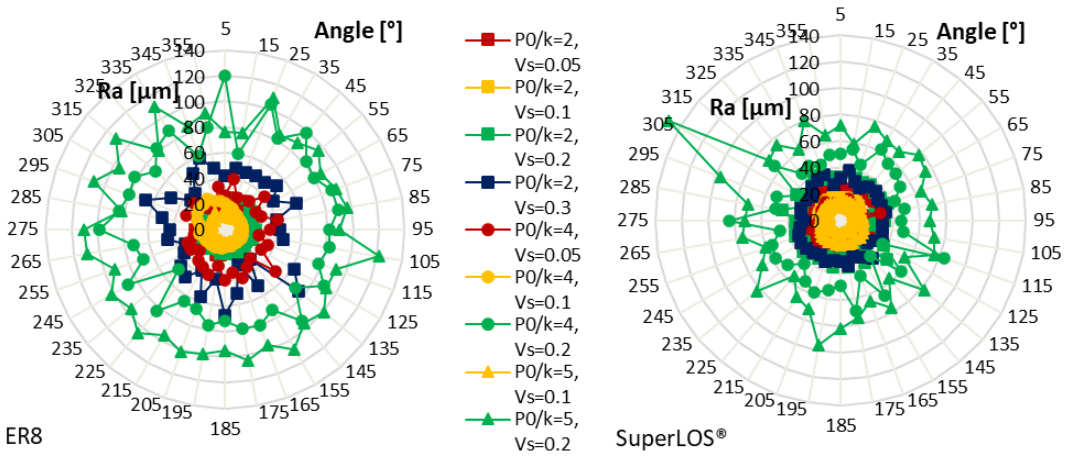

Figure 8: Quadratic roughness of the wheel specimens along the circumference.

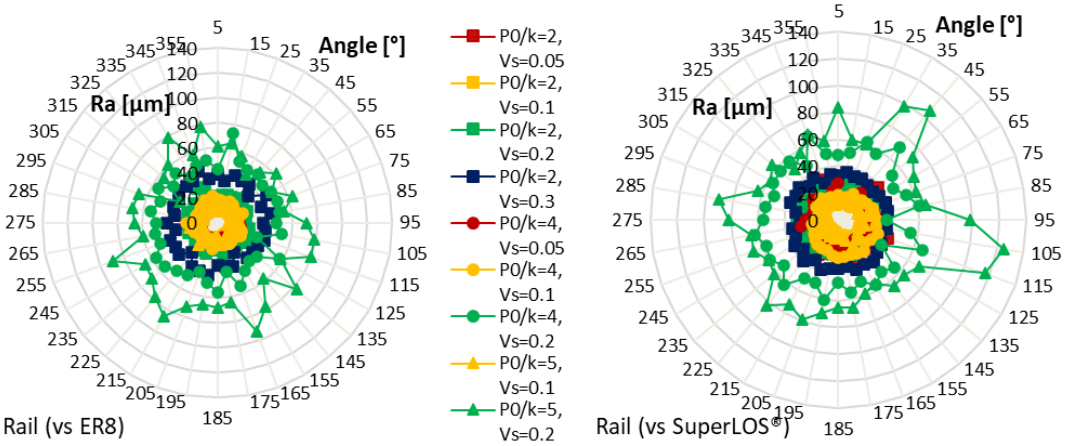

Figure 9: Quadratic roughness of the rail specimens along the circumference.

The measured weight loss is shown in Figure 10 for both the wheel rail specimens. The reported measurements are the average result of three weightings done at the end of each session; the initial weight was measured at the end of the run-in session. The most influencing parameter is the sliding speed, because for $Vs = 0.2$ m/s and $Vs = 0.3$ m/s the weight loss is at least one magnitude higher than in the other cases. At high sliding speed, the weight loss in the wheel specimens is higher than in the rail ones, and in the ER8 specimens higher than in the SUPERLOS® ones.

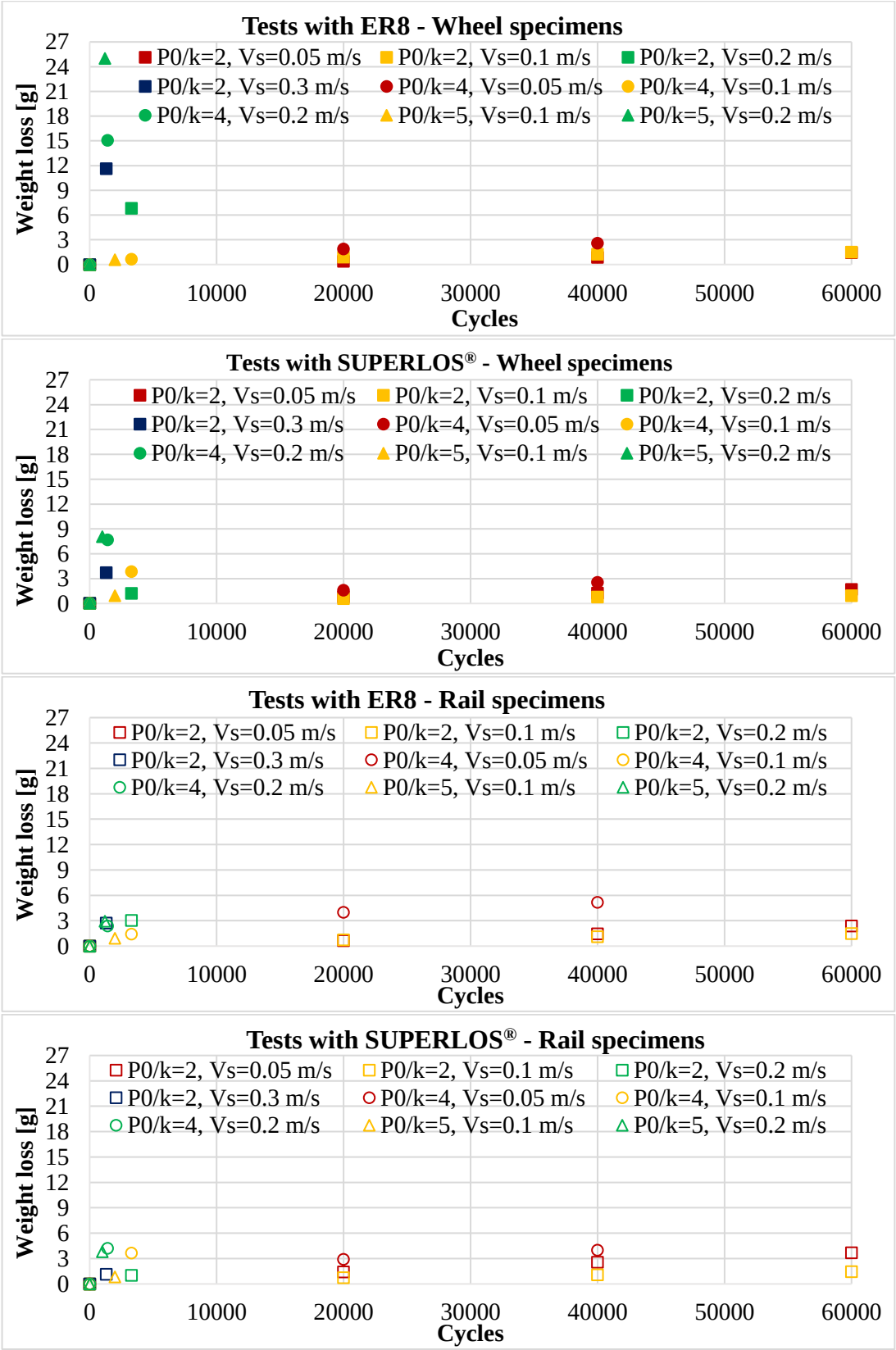

Figure 10: Weight loss in wheel and rail specimens.

To characterize the wear behavior, the Archard wear number K was calculated, according to the following relationship:

$$K = \frac{\Delta V \cdot H}{F \cdot \Delta s} \quad (1)$$

where:

- ΔV is the worn volume;
- H is the Brinell hardness of the softer material, that in the present work is the wheel steel;
- F is the normal contact load;
- Δs is the sliding distance.

In addition, for each test the $T\gamma/A$ parameter was calculated according to the specific "*T-gamma*" model, where:

- T is the tangential load, calculated multiplying the normal load by the average coefficient of friction;
- γ corresponds to the creepage c expressed as pure number (not as percentage);
- A is the nominal contact area.

In Figure 11 the wear number K for both wheel and rail materials in the various test conditions is shown. In Figure 12 the wear number K as a function of $T\gamma/A$ is given for the wheel specimens; the regions where wear is classified as "mild", "severe" or "catastrophic" [11], based on the wear number, are also identified. In Figure 13 the same data for the rail specimens are given. Considering the wheel specimens, the ER8 ones undergo catastrophic wear in all tests where the sliding speed is equal to or higher than 0.2 m/s, independently of the applied pressure. For the SUPERLOS® the same considerations apply, except for the case with $P0/k = 2$ and $Vs = 0.2\ \mathrm{m/s}$, which causes severe wear instead of catastrophic. Considering the rail specimens, catastrophic wear occurred less frequently than for the wheel ones.

All these results agree with what was highlighted by the weight loss and roughness analyses, e.g. that:

- the most influencing parameter for wear is the sliding speed;
- wear is higher in the wheel specimens than in the rail ones;
- the SUPERLOS® steel has a wear resistance higher than the ER8 one.

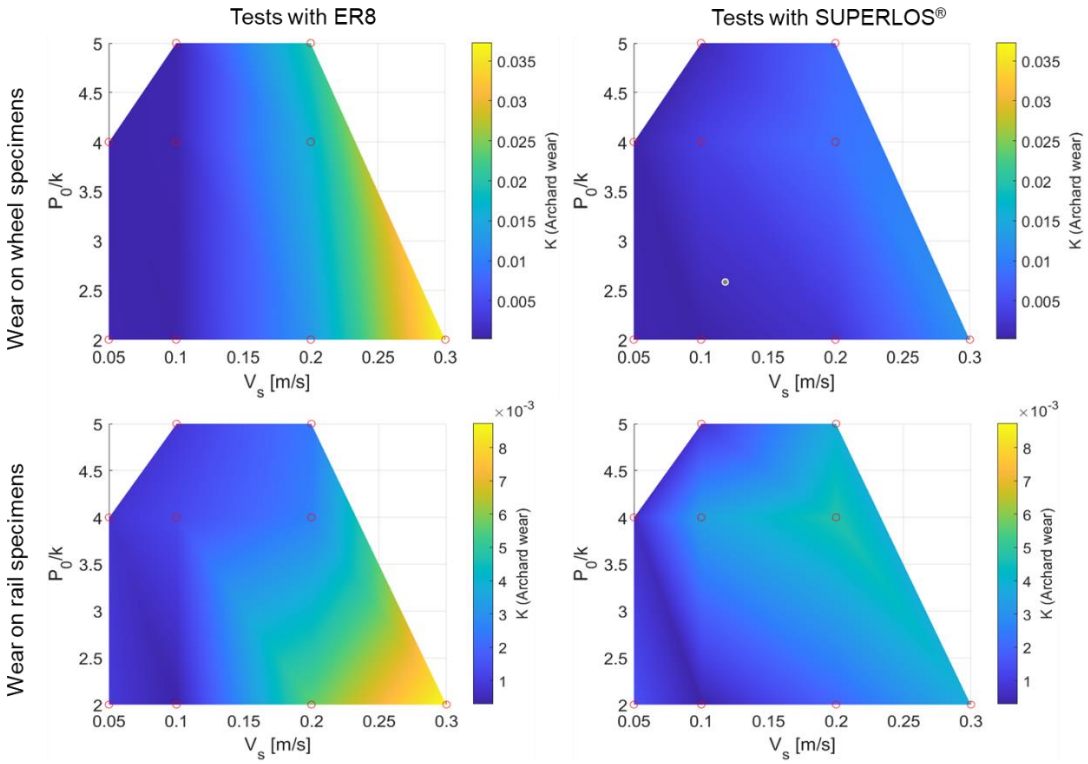

Figure 11: Wear number in wheel and rail specimens.

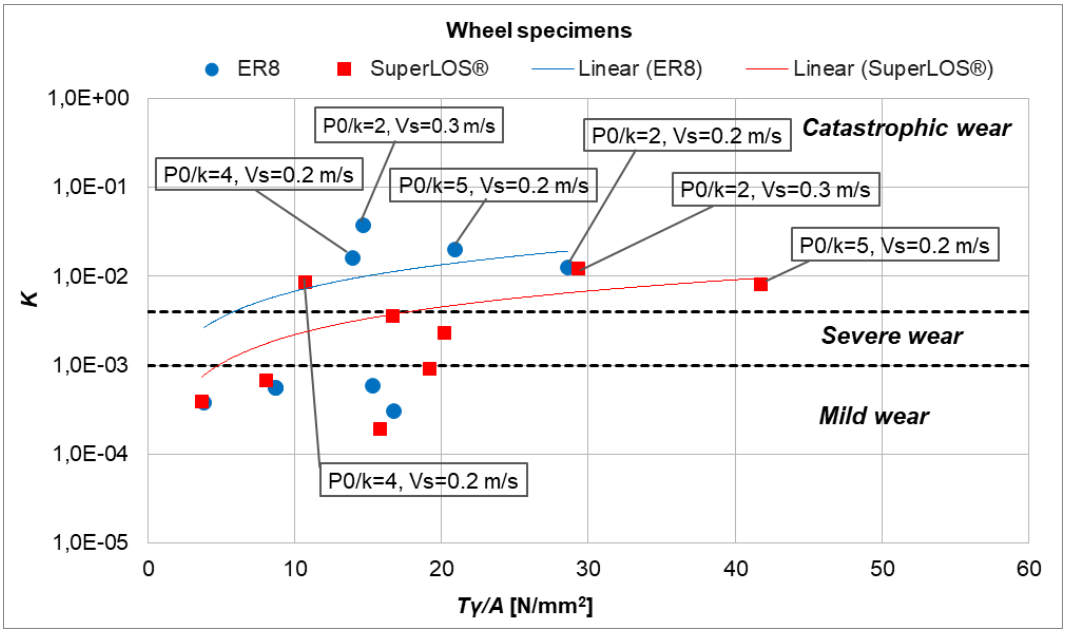

Figure 12: Wear number as a function of $T\gamma/A$ in wheel specimens.

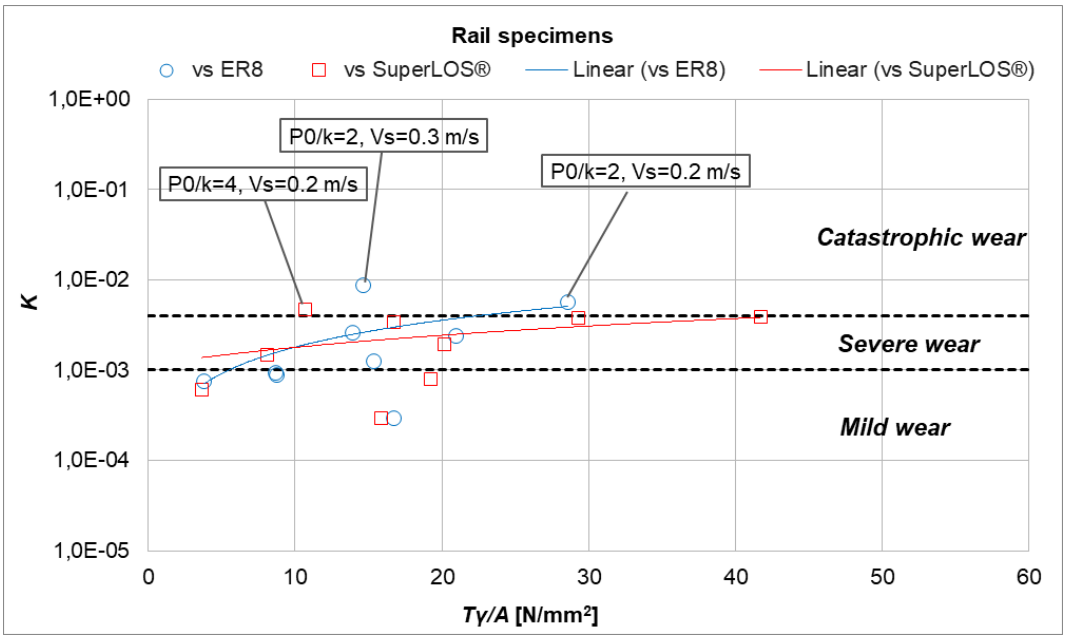

Figure 13: Wear number as a function of $T\gamma/A$ in rail specimens.

4 Conclusions

Rolling and sliding contact tests were carried out on couples of wheel-rail steels, with varying contact pressure and sliding speed, up to very harsh conditions. Two railway wheel steels (ER8 and SUPERLOS®) were tested against the same rail steel (900A). Measurements of the coefficient of friction and wear rate were taken; in addition, the roughness of the contact surfaces was measured by an innovative vision system.

The main obtained results are the following:

- the roughness at the end of the tests is influenced by both the contact pressure and the sliding speed, but the latter has more weight in determining the damage severity;
- wear tends to become catastrophic in the wheel steels when the sliding speed exceeds 0.2 m/s;
- among the wheel steels, the SUPERLOS® exhibits a better wear resistance;
- the wheel steels wear out more than the rail steel.

The results also showed a strong correlation between the roughness measured with the vision system and wear rate, suggesting it can be used as an effective diagnostic tool for the surface damage.

Acknowledgements

The authors would like to thank Lucchini RS for the technical and financial support, and Prof. Stefano Bruni of the Politecnico di Milano for the collaboration in conceptualization and planning.

References

[1] B. Wu, G. Xiao, B. An, T. Wu, Q. Shen, “Numerical study of wheel/rail dynamic interactions for high-speed rail vehicles under low adhesion conditions during traction”, Engineering Failure Analysis, 137, 106266, 2022.

[2] Y. Özdemir, P. Voltr, “Analysis of wheel-rail contact under partial slip and low speed conditions”, Mechanika, 23(1), 5-10, 2017.

[3] T. Telliskivi, U. Olofsson, “Wheel–rail wear simulation”, Wear, 257, 1145-1153, 2004.

[4] J. Liu, Y. Li, Y. Zhang, Y. Hu, L. Shi, H. Ding, W. Wang, F. Liu, S. Zhou, and T. Shi, “Dry rolling/sliding wear of bainitic rail steels under different contact stresses and slip ratios”, Materials, 13, 4678, 2020.

[5] S. Pal, W.J.T. Daniel, C.H.G. Valente, A. Wilson, A. Atrens, “Surface damage on new AS60 rail caused by wheel slip”, Engineering Failure Analysis, 22, 152-165, 2012.

[6] R. Lewis, U. Olofsson, “Mapping rail wear regimes and transitions”, Wear, 257, 721-729, 2004.

[7] D.H. Mesa G., I. Alari Vasquez-Chacon, M.A. Gomez–Guarneros, P. Sanchez-Tizapantzi, E.A. Gallardo-Hernandez, “A pin-on-disk wear map of rail and wheel materials from different standards”, Materials Letters, 307, 13102, 2022.

[8] N. Zani, C. Petrogalli, “Predictive maps for the rolling contact fatigue and wear interaction in railway wheel steels”, Wear, 510-511, 204513, 2022.

[9] G. Donzella, M. Faccoli, A. Mazzù, C. Petrogalli, R. Roberti, “Progressive damage assessment in the near-surface layer of railway wheel–rail couple under cyclic contact”, Wear, 271, 408-416, 2011.

[10] I. Bodini, C. Petrogalli, M. Faccoli, M. Lancini, S. Pasinetti, G. Sansoni, F. Docchio, A. Mazzù, “Evaluation of wear in rolling contact tests by means of 2D image analysis”, Wear, 400-401, 156-168, 2018.

[11] T. Jendel, “Prediction of wheel profile wear-comparisons with field measurements”, Wear, 253, 89-99, 2002.